RESEARCH PAPER

Replacing friction model with interaction between particles in analyzing orthogonal and rotational cutting processes using SPH method

Mohammad Dehghani, Alireza Shafiei∗

Department of mechanical Engineering, Yazd University, Yazd, Iran

Abstract

The cutting tool and work-piece of cutting process are commonly analyzed using Finite Element (FE) and Smooth-Particle Hydrodynamics (SPH) methods respectively. This is identified a compound method in this research. The interaction between cutting tool elements and work-piece particles are modeled as pressure and friction force. The coefficient of friction (CF) between cutting tool and work-piece is the fundamental parameter of friction model. The CF effects on chip morphology and cutting force. In present study, both cutting tool and work-piece of cutting process are analyzed using SPH method without Friction and pressure model (SPH.NO.F). Therefore the pressure and friction force between elements and particles in compound method are replaced with the interaction between particles. The friction in the cutting zones is a physical process that accompanies the cutting but this is not modeled in analyzing of this process, because the cutting tool and work-piece particles interact with each other using the mass and momentum conservation equation. The results of orthogonal cutting process show the chip morphology of SPH.NO.F method is the same as compound method with friction model by CF=0 and 0.17. The cutting force of SPH.NO.F method is coincided to experimental results. The cutting force of rotational process is investigated using SPH.NO.F and compound method by CF=0 and 0.17.

Keywords:

 replacing friction model; orthogonal cutting; rotational cutting; SPH method

1. Introduction

The CF is an unknown parameter while analysing orthogonal cutting process using numerical methods like FEM and SPH method.

Zhang et al. [1] investigated a new friction model at tool-chip interface in dry orthogonal cutting based on theoretical analysis and used the experimental results of AISI 1050 steel and TiAlN coating tool to validate this model. In their modelling, local normal stress decreases along the tool rake face. Cakir et al. [2] investigated of temperature distribution of the orthogonal cutting process using a two-dimensional analytical model. The contact forces were obtained by modelling sticking and sliding friction zones on rake face. Asad et al. [3] studied dry cutting of aluminium alloy (A2024-T351) using FEM. They simulated a 2-D orthogonal cutting model with plane strain assumption using Abaqus/Explicit. Calamaz et al. [4] investigated machining titanium alloys with a new material constitutive behaviour in a 2D finite element model. They used commercial finite element software (FORGE 2005s) to solve this thermo-mechanical problem. The tool chip friction was modelled by a combined Coulomb–Tresca friction law. Maranhao et al. [5] simulated the thermo-mechanical treatment of machining a stainless steel (AISI 316) and investigated the influence of the friction coefficient in the tool-chip interface on cutting and feed forces, cutting temperature, plastic strain, plastic strain rate, maximum shear stress and residual stresses. They used commercial

---

∗ Corresponding Author. Tel.: +983531232496; Fax: +983538212781
Email Address: arshafiei@yazd.ac.ir

software Advantedge[TM] to aid this study and Coulomb friction coefficient equal to 0.89, 0.80 and 0.53 while feed rate was 0.05, 0.1 and 0.2 (mm/rev) respectively.

The SPH has not the disadvantages of FEM such as large deformations and material separation. This method is based on displacement and acceleration of work-piece particle. Basic SPH method has been investigated by Monaghan [6] for the first time and now it is used to solve Fluid and solid mechanics [7–9] such as crack [10], elastic [11] and plastic [12] deformations. Takabi et al. [13] compared results of smoothed particle hydrodynamics method and finite element method in orthogonal cutting simulations. They showed stress increases until the element distortion crashes the simulation using undamageable FEM model, but undamageable SPH can simulate this process because of natural particles separation when the progressive damage of the material takes into account. SPH does not produce a continuous curled chip as FEM typically does. Geng et al. [14] simulated the orthogonal cutting of OFHC copper based on the smoothed particle hydrodynamics method using commercial software of company LSTC [15]. Nam et al. [16] numerically investigated the cutting process of brittle materials using SPH method. They optimized cutting conditions by affecting various parameters like cutting speed, cutting depth and rake angle on the surface roughness. Avachat and Cherukuri [17] studied the effect of the three parameters like the smoothing length, particle density, and the type of SPH formulation (classical, renormalization and total Lagrangian formulations) using The LS-DYNA FE package. They introduced the model with variable smoothing length of particles and renormalization SPH formulations include the most efficient results as chip morphology. The work-piece can be model with combination of FE and SPH method. This refers to feed and other part of work-piece can be model with SPH and FE method respectively. Xi et al. [18] used these methods and thermal solution to simulate of cutting force and chip formation during machining of Ti6Al4V alloy. The chip isn't curled, and the cutting force is significant while a saw-tooth of the chip is fully generated in primary zone and it will start to decrease when the crack propagates inside the primary deformation zone. In many researches the tool is modelled as a rigid body because its deformation is extremely insignificant with contrast to chip formation. Therefore, the cutting wears cannot be investigated following this rigid model. Calamaz [19] obtained the shape of new and worn tool tip by capturing the photo of tool tip before and after orthogonal machining experimentally. Then simulated these cutting processes with two different tool tip and compared the experimental and numerical cutting force together to demonstrate ability of SPH method in simulating of this process. Niu et al. [20] simulated orthogonal cutting process of A2024-T351 with an improved SPH method. The improved SPH method is achieved by density and kernel gradient correction. Spreng et al. [21] modelled orthogonal metal cutting using adaptive SPH (ASPH). In ASPH method the smoothing length of any SPH particles vary by time. In their research the rigid boundaries are modelled with modified Lennard-Jones penalty force function [22]. Umer et al. [23] modelled serrated chip formation in hardened steel using FEM, SPH and renormalized SPH (RSPH). They used the LS-DYNA to simulate the cutting process in which the RSPH formulation is based on the work of Randles and Libersky [9] and Vila [24].

To the best of author's knowledge, all researches use the friction model to control the contact interface between tool and work-piece. If the tool and work-piece are analysed using FEM and SPH method respectively then the unknown coefficient of friction causes uncertainly results. In this research, cutting tool and work-piece of cutting process are both analysed using SPH.NO.F method. Therefore, this simulation does not need the modelling of friction. The orthogonal and rotational cutting processes are analysed using SPH.NO.F method. The results of this analysing is compared with compound method while CF=zero and 0.17. Furthermore, the cutting force of orthogonal cutting process is near the experimental result.

2. SPH formulation for solid flows

The integral approximation of the function f(x) at x_i in *SPH* is [25]:

$$f\left(x_i\right) \approx \int_\Omega f\left(x\right) w\left(x - x_i\right) dA$$

(1)

Where Ω is integration area, *W* is a kernel function that is shown in Fig. 1.
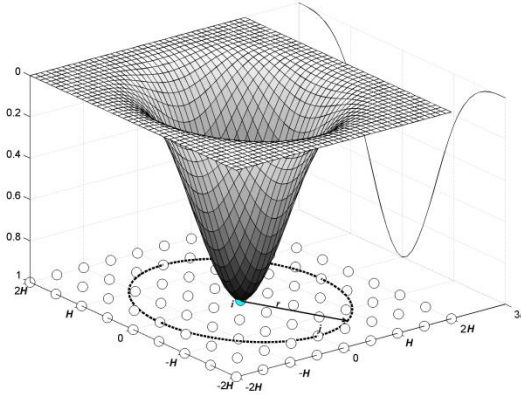
Fig. 1. Kernel function at particle i and its neighbors (j)

The derivative of the Eq. (1) is:

$$\frac{\partial f\left(x_i\right)}{\partial x} \approx -\int_{\Omega} f\left(x\right) \frac{\partial w\left(x - x_i\right)}{\partial x} dA$$

(2)

And discrete form of Eq. (2) is:

$$\frac{\partial f\left(x_i\right)}{\partial x} = -\sum_{j \in \Omega} f_j \frac{\partial w\left(x - x_i\right)}{\partial x} A_j$$

(3)

Therefore derivative of the function f at x_i of particle i is approximated by summing the f_j the value of function f at particle j as the neighbor of particle i, A_j is area of a particle and equals to m_j/ρ_j, m_j and ρ_j are mass and density of particle j respectively. As the definition of A_j the Eq. (3) is changed to Eq. (4).

$$\frac{\partial f\left(x_i\right)}{\partial x} = -\sum_{j \in \Omega} f_j \frac{\partial w_{ij}}{\partial x} \frac{m_j}{\rho_j}$$

(4)

Where $W_{ij} = W(x_i - x_j)$.
The mass and momentum conservation are Eq. (5) and Eq. (6) respectively.

$$\frac{d\rho}{dt} = \rho \frac{\partial V_\beta}{\partial X_\beta} \qquad \beta = 1,2$$

(5)

$$\frac{dV_\alpha}{dt} = \frac{1}{\rho} \frac{\partial \sigma_{\alpha\beta}}{\partial X_\beta} \qquad \alpha = 1, 2$$

(6)

Where t is time, V is velocity, σ is stress and
$V = [V_1\ V_2] = [u\ v]$
$X = [X_1\ X_2] = [x\ y]$
$$\begin{bmatrix} \sigma_1 & \sigma_{12} \\ \sigma_{12} & \sigma_2 \end{bmatrix} = \begin{bmatrix} \sigma_x & \sigma_{xy} \\ \sigma_{xy} & \sigma_y \end{bmatrix}$$

(7)

The mass conservation equation can be formulated as in Eq. (8)

$$\frac{d\rho}{dt} = -\frac{\partial\left(\rho V_\beta\right)}{\partial X_\beta} + V_\beta \frac{\partial\left(\rho\right)}{\partial X_\beta}$$

(8)

The discrete form of Eq. (8) is shown in Eq. (9) using particle approximation of Eq. (4).

$$\frac{d\rho_i}{dt} = -\sum_j \rho_j V_\beta^j \frac{\partial W_{ij}}{\partial X_\beta} \frac{m_j}{\rho_j} + V_\beta^i \sum_j \rho_j \frac{\partial W_{ij}}{\partial X_\beta} \frac{m_j}{\rho_j}$$
$$= \sum_j m_j \left(V_\beta^i - V_\beta^j\right) \frac{\partial W_{ij}}{\partial X_\beta}$$

(9)

Therefore the discrete form of mass conservation equation is:

$$\frac{d\rho_i}{dt} = \sum_{j \in \Omega} m_j \left(V_\beta^i - V_\beta^j\right) \frac{\partial W_{ij}}{\partial X_\beta}$$

(10)

The discrete form of Eq. (6) is shown in Eq. (11) using particle approximation of Eq. (4).

$$\frac{dV_\alpha^i}{dt} = \frac{1}{\rho_i} \sum_{j \in \Omega} \sigma_{\alpha\beta}^j \frac{\partial W_{ij}}{\partial X_\beta} \frac{m_j}{\rho_j}$$

(11)

If the acceleration of Eq. (11) is multiply with the mass of particle i then the force of this particle is:

$$F_{ij}^\alpha = \frac{m_i}{\rho_i} \sigma_{\alpha\beta}^j \frac{\partial W_{ij}}{\partial X_\beta} \frac{m_j}{\rho_j}$$

(12)

Eq. (12) doesn't satisfy the third Newton's law. The discrete form of derivation of function f=1 is added to Eq. (11) as below:

$$0 = \frac{d1}{dX_\beta} = \sum_j (1) \frac{\partial W_{ij}}{\partial X_\beta} \frac{m_j}{\rho_j} = \frac{\sigma_{\alpha\beta}^i}{\rho_i} \sum_j \frac{\partial W_{ij}}{\partial X_\beta} \frac{m_j}{\rho_j}$$

(13)

Therefore the discrete form of momentum conservation equation is:

$$\frac{dV_\alpha^i}{dt} = \sum_{j \in \Omega} m_j \left(\frac{\sigma_{\alpha\beta}^i + \sigma_{\alpha\beta}^j}{\rho_i \rho_j}\right) \frac{\partial W_{ij}}{\partial x_\beta}$$

(14)

Eq. (14) satisfied the third Newton's law as $F_{ij}^\alpha = -F_{ji}^\alpha$. The strain rate at particle i is expressed as follow:

$$\dot{\varepsilon}_{\alpha\beta}^i = \frac{1}{2}\left(\frac{\partial V_\alpha^i}{\partial X_\beta} + \frac{\partial V_\beta^i}{\partial X_\alpha}\right)$$

(15)

Where

$$\frac{\partial V_\alpha^i}{\partial X_\beta} = \sum_{j \in \Omega} \frac{m_j}{\rho_j} \left(V_\alpha^j - V_\alpha^i\right) \frac{\partial W_{ij}}{\partial X_\beta}$$

(16)

3. Model configurations

Fig. 2 (a) shows an orthogonal cutting process. The horizontal and vertical displacements of the right boundary are zero. At this Figure the cutting speed is V_c=800 (m/min), work-piece dimensions are L×H and feed rate is f=0.4 (mm/rev), the rake angle is equal to 17.5° and the depth of cut is equal to 4mm for an aluminium of type A2024-T351 with the yield stress 440 (MPa) [26]. Fig. 2 (b) shows an entering of cutting tool tip to the work-piece at the rotational cutting process. The horizontal and vertical displacements of left, bottom and right boundaries are fixed. The tool turns with constant angular velocity ω around fixed point O while the tangential velocity of cutting tool tip is equalled to 19.89 (m/s), the radial depth is 0.2 (mm) and the depth of cut is equal to 0.1 (mm).

<div align="center">(a)</div>
<div align="center">(b)</div>
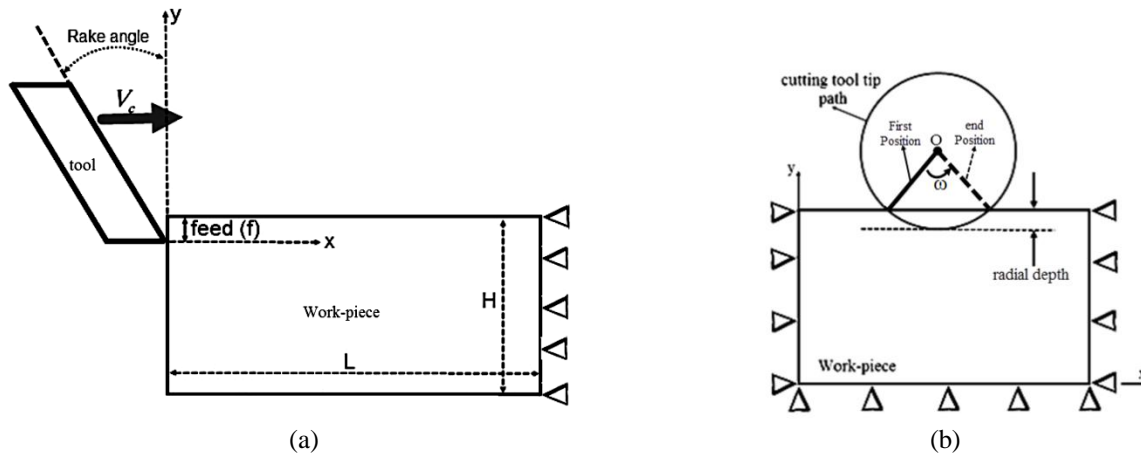
Fig. 2. The boundary condition of (a) orthogonal (b) rotational cutting process

The cutting parameters of orthogonal and rotational cutting processes are listed at table 1.

Table 1. Cutting conditions

Cutting condition	
orthogonal cutting process	
cutting speed	800 (m/min)
feed rate	0.4 (mm/rev)
rake angle	17.5°
depth of cut	4 (mm)
rotational process	
radial depth	0.2 (mm)
depth of cut	0.1 (mm)

According to Fig. 2 (a) the work-piece and cutting tool are discretized by a set of particles as Fig. 3 (a). The second numerical model of Fig. 2 (a) is shown at Fig. 3 (b). The cutting tool and work-piece are analysed using FE and SPH method respectively. The friction between these parts is modelled as Coulomb's Friction law while the coefficient of friction is equalled to zero and 0.17.

<div align="center">(a) SPH.NO.F method</div>
<div align="center">(b) Compound method (FE and SPH)</div>
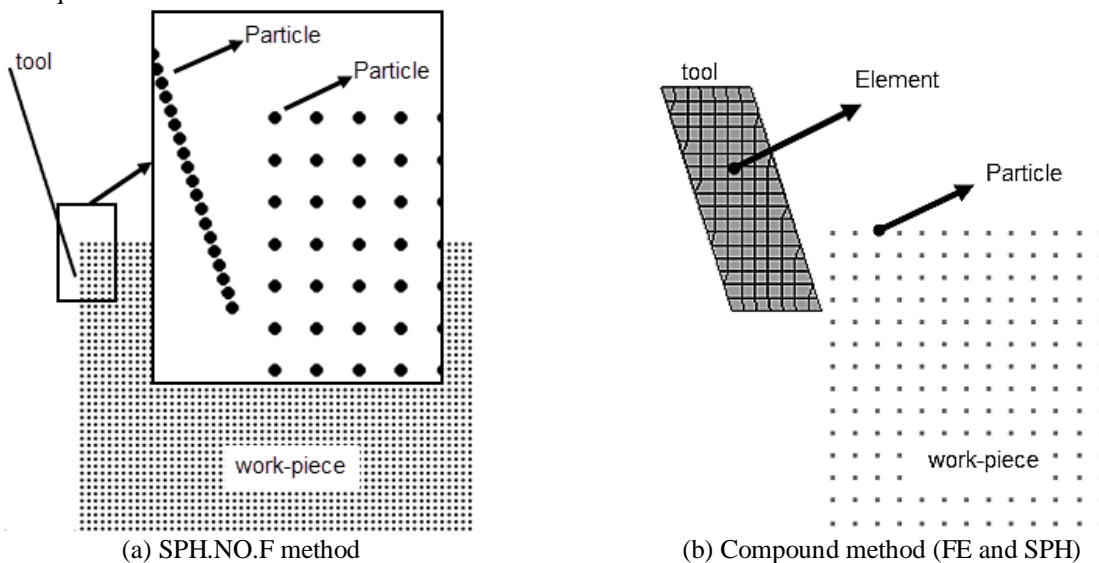
Fig. 3. (a) Analysing work-piece and cutting tool using SPH particles (b) Analysing work-piece and cutting tool using SPH particles and elements respectively.

If the cutting tool and work-piece of Fig. 2 (b) are both analyzed using SPH method then the configuration of model is shown at Fig. 4 (a). If the cutting tool and work-piece are analyzed using FEM and SPH method respectively then the configuration of model at LS-DYNA software is shown at Fig. 4 (b).

(a) SPH.NO.F method   (b) Compound method (FE and SPH)
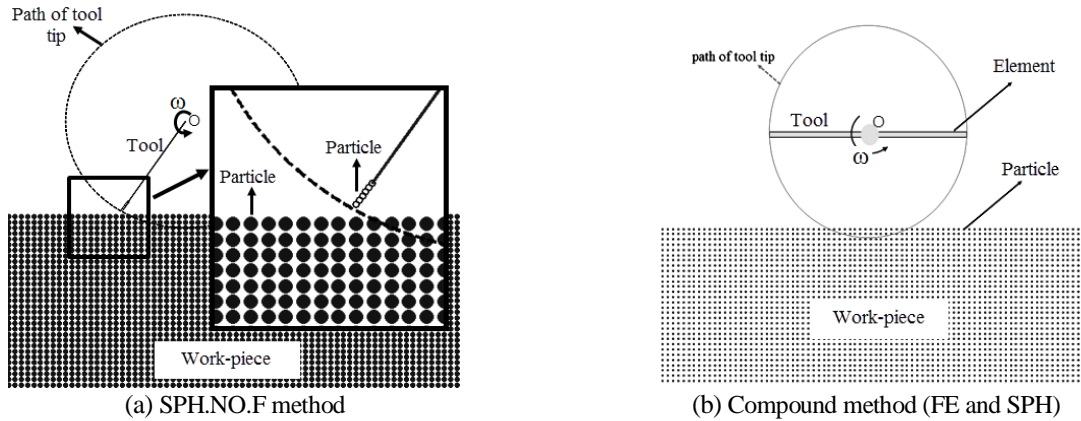
Fig. 4. Model configuration of rotational cutting process while (a) the cutting tool and work-piece are analyzed using SPH method (b) the cutting tool and work-piece are analyzed using FEM and SPH method respectively.

The mechanical properties of the cutting tool and work-piece are listed at table 2. The aluminium particles are used to model the rake face. It doesn't mean the tool is also made of aluminium A2024-T351 because the cutting tool is a rigid body. Based on rigid assumption, these tool particles don't move with respect to each other and always fix on the rake face. These tool particles transfer force displacement of the cutting tool to the work-piece particles.

Table 2. Mechanical properties of cutting tool and work-piece

properties	work-piece	cutting tool
Modulus of elasticity(GPa)	73	534
Density (kg/m^3)	2700	11900
Poison ratio	0.33	0.22
Yield stress(MPa)	440	-

The perfectly elastic-plastic material model is applied to simulate the aluminium behaviour during the cutting process using SPH.NO.F and compound methods. The von-Mises yield criterion is used to identify the critical point of plastic deformation. In SPH.NO.F simulation, the von-Mises stress (σ_{von}) is compared to the flow yield stress (S_y), and when the criterion ($\sigma_{von} \geq S_y$) is satisfied, the material enters plastic deformation (flow).

4. Results and Discussion

In this section the chip morphology, cutting force and velocity distribution of the particle are presented. The cutting force of the orthogonal cutting process is validated with experimental result [26].

Chip morphology of orthogonal cutting process after 0.2 msec at cutting speed of 800 m/min is shown at Fig. 5. At this figure chip shape using compound method with the coefficient of friction and SPH.NO.F are shown. The CF is equal to zero and 0.17. The results of SPH.NO.F method confirms the compound method, because the chip thicknesses approximately are same and the length of the chip is between the results of compound method. The CF=zero is the longest chip because the reaction of rake face is lowest one.
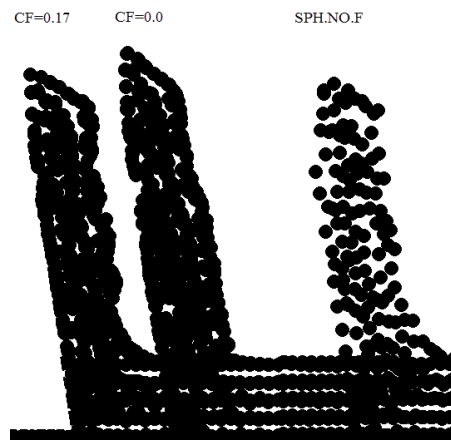
Fig. 5. Chip morphology of orthogonal cutting process using SPH and SPH.NO.F at 800 m/min cutting speed

An average curve for cutting force of orthogonal cutting process is derived from oscillatory results using curve fitting as Fig. 6 to compare the cutting forces of different methods. These methods are experimental [26], compound method with two various coefficient of friction (CF=0 and 0.17) and SPH.NO.F.
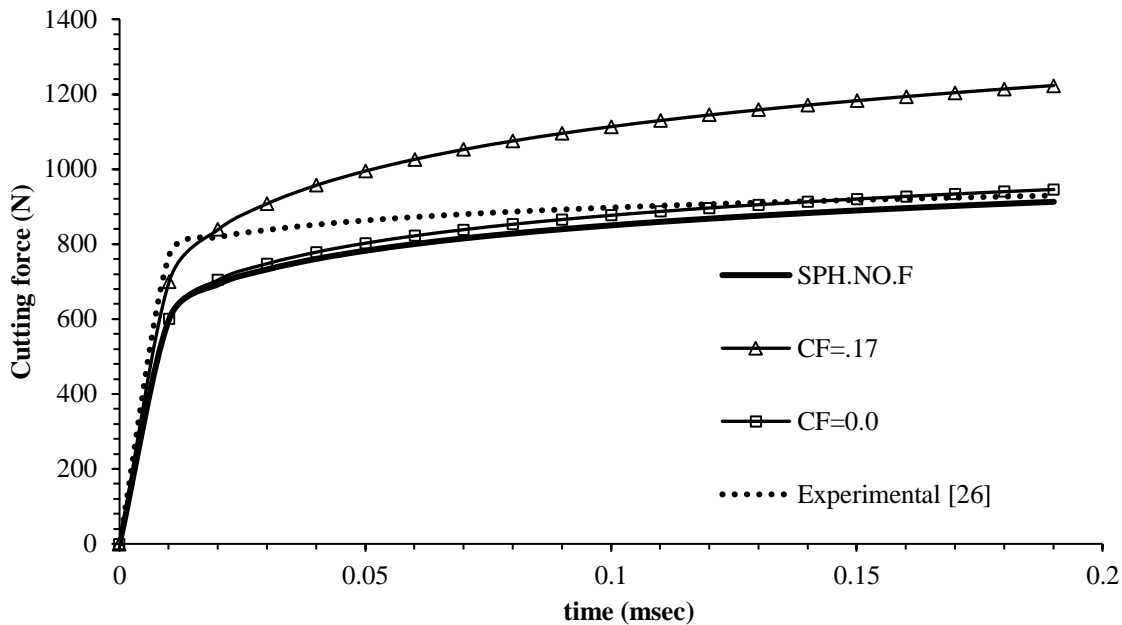
Fig. 6. Experimental cutting force of orthogonal cutting process [26] at speed of 800 m/min and results of simulation using compound and SPH.NO.F method

According to Fig. 6, the cutting force increases by increasing coefficient of friction from zero to 0.17 using compound method. The cutting force of compound method with CF=0 and SPH.NO.F are same as experimental results.

To illustrate the chip condition of orthogonal cutting process at some points of cutting force at last figure, the absolute speed of particles along cutting direction at 0.05, 0.14 and 0.2 msec are shown at Fig. 7. These results are obtained using SPH.NO.F method.
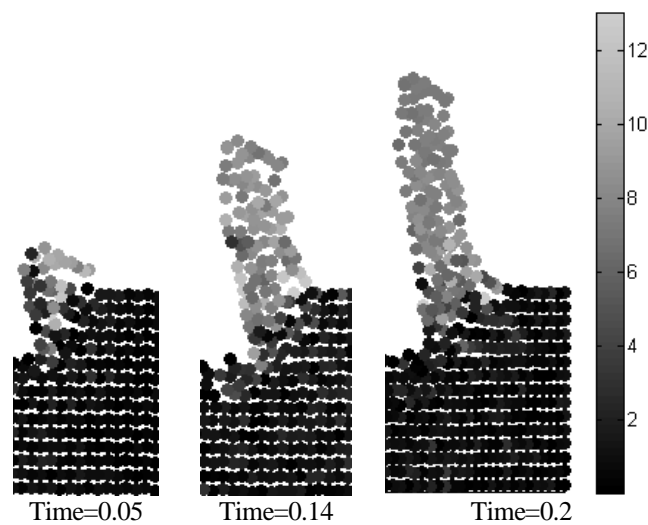
Fig. 7. Speed of work-piece particle along cutting direction of orthogonal cutting process at 800 m/min cutting speed

The cutting force along horizontal direction of rotational process is plotted at Fig. 8 from entering the cutting tool to the work-piece to exiting time. The cutting forces at this figure are investigated using compound and SPH.NO.F method. The coefficients of friction are equal zero and 0.17.
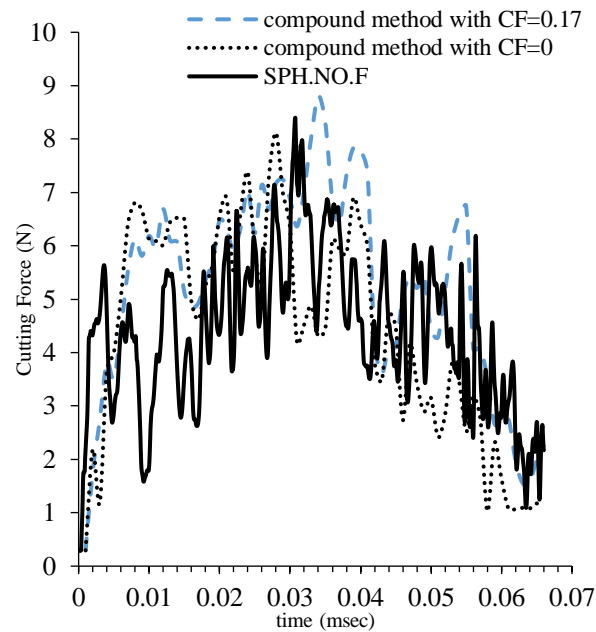
Fig. 8. Cutting force of rotational process along horizontal direction from entering cutting tool to the work-piece to exiting time

Approximate second order polynomials of cutting forces at Fig. 8 are plotted at Fig. 9 to compare the cutting forces. According to Fig. 9, the SPH.NO.F cutting force is lower than others at half of the cutting process but it is higher than CF=0 at other part of process. Maximum cutting force of SPH.NO.F and compound method with CF=0.17 occur simultaneously, but the maximum force of CF=0 is at the sooner time. The cutting force of CF=0 and 0.17 are relatively equal at the start of the process, but the force of CF=0.17 is becoming additionally than CF=0 by time increasing.
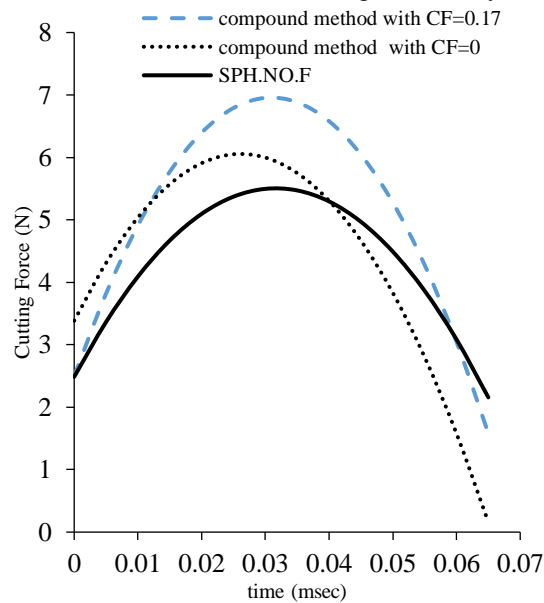
Fig. 9. Average cutting force of Fig. 8 using curve fitting with second order polynomials

5. Conclusions

In this paper, tool and work-piece of the orthogonal and rotational cutting processes were both analysed using SPH method. Therefore, the friction coefficient was not required.

Cutting force and chip morphology were obtained using SPH.NO.F. These results were compared to results of

orthogonal cutting process simulation using compound method with CF equal to zero and 0.17. The cutting force of SPH.NO.F method is unique and it is coinciding to the experimental results. The cutting force of compound method varies by applying different CF.

The SPH.NO.F cutting force of rotational process is lower than others at first half of the cutting process but it is higher than CF=0 at second half of process.

References

[1]   Zhang C, Lu J, Zhang F, Ikramullah S. 2017. Identification of a new friction model at tool-chip interface in dry orthogonal cutting. Int J Adv Manuf Technol 89:921–932.

[2]   Cakir E, Ozlu E, Bakkal M, Budak E. 2018. Investigation of temperature distribution in orthogonal cutting through dual-zone contact model on the rake face. Int J Adv Manuf Technol 96:81–89.

[3]   Asad M, Girardin F, Mabrouki T, Rigal J-F. 2008. Dry cutting study of an aluminium alloy (A2024-T351): a numerical and experimental approach. Int J Mater Form 1:499–502.

[4]   Calamaz M, Coupard D, Ã FG. 2008. A new material model for 2D numerical simulation of serrated chip formation when machining titanium alloy Ti – 6Al – 4V. Int J Mach Tools Manuf 48:275–288.

[5]   Maranhão C, Davim JP. 2010. Simulation Modelling Practice and Theory Finite element modelling of machining of AISI 316 steel : Numerical simulation and experimental validation. Simul Model Pract Theory 18:139–156.

[6]   Monaghan JJ. 1992. Smoothed Particle Hydrodynamics. Annu Rev Astron Astro-physics 30:543–574.

[7]   Benz W, Asphaug E. 1995. Simulations of brittle solids using smooth particle hydrodynamics. Comput Phys Commun 87:253–265.

[8]   Monaghan JJ. 2012. Smoothed Particle Hydrodynamics and Its Diverse Applications. Annu Rev Fluid Mech 44:323–346.

[9]   Randles P, Libersky LD. 1996. Smoothed particle hydrodynamics: some recent improvements and applications. Comput methods Appl Mech 139:375–408.

[10]   Cleary PW, Das R. 2008. The Potential for SPH Modelling of Solid Deformation and Fracture. In: IUTAM Symp. Theor. Comput. Model. Asp. Inelast. Media. pp 287–296.

[11]   Gray JP, Monaghan JJ, Swift RP. 2001. SPH elastic dynamics. Comput Methods Ap-plied Mech Eng 190:6641–6662.

[12]   Hiermaier S, Konke D, Stilp AJJ, Thoma K, Könke D. 1997. Computational simulation of the hypervelocity impact of al-spheres on thin plates of different materials. Int J Impact Eng 20:363–374.

[13]   Takabi B, Tajdari M, Tai BL. 2017. Numerical study of smoothed particle hydrodynamics method in orthogonal cutting simulations – Effects of damage criteria and particle density. J Manuf Process 30:523–531.

[14]   Geng X, Dou W, Deng J, Ji F, Yue Z. 2017. Simulation of the orthogonal cutting of OFHC copper based on the smoothed particle hydrodynamics method. Int J Adv Manuf Technol 91:265–272.

[15]   2007. LS-DYNA Keyword User's Manual. .

[16]   Nam J, Kim T, Cho SW. 2016. A numerical cutting model for brittle materials using smooth particle hydrodynamics. Int J Adv Manuf Technol 82:133–141.

[17]   Avachat CS, Carolina N, Carolina N. 2015. A Parametric Study of the Modeling of Orthogonal Machining. In: Proc. ASME 2015 Int. Mech. Eng. Congr. Expo. pp 1–10.

[18]   Xi Y, Bermingham M, Wang G, Dargusch M. 2014. SPH / FE modeling of cutting force and chip formation during thermally assisted machining of Ti6Al4V alloy. Comput Mater Sci 84:188–197.

[19]   Calamaz M, Limido J, Nouari M, Espinosa C, Coupard D, Salaün M, Girot F, Chieragatti R. 2009. Int . Journal of Refractory Metals & Hard Materials Toward a better understanding of tool wear effect through a comparison between experiments and SPH numerical modelling of machining hard materials. Int J Refract Met Hard Mater 27:595–604.

[20]   Niu W, Mo R, Liu GR, Sun H, Dong X. 2018. Modeling of orthogonal cutting process of A2024-T351 with an improved SPH method. Int J Adv Manuf Technol 95:905–919.

[21]   Spreng F, Eberhard P. 2018. Modeling of Orthogonal Metal Cutting Using Adaptive Smoothed Particle Hydrodynamics. In: Biermann D., Hollmann F. (eds) Thermal Effects in Complex Machining Processes. Lecture Notes in Production Engineering. Springer, Cham. pp 133–143.

[22]   Müller M, Schirm S, Teschner M, Heidelberger B, Gross M. 2004. Interaction of fl uids with deformable solids. J Vis

Comput Animat 15:159–171.

[23]   Umer U, Mohammed MK, Qudeiri JA. 2016. Assessment of finite element and smoothed particles hydrodynamics methods for modeling serrated chip formation in hardened steel. Adv Mech Eng 8:1–11.

[24]   Vila JP. 2006. SPH renormalized hybrid methods for conservation laws: applications to free surface flows. In: Meshfree Methods Partial Differ. Equations II. Lecture Notes in Computational Science and Engineering, pp 207 – 229.

[25]   Liu GR, Liu MB. 2003. Smooth Particle Hydrodynamics : a mesh free particle method . World Scientific, 5 Toh Tuck Link, Singapore 596224, ISBN 9789812384560.

[26]   Madaj M, Píška M. 2013. On the SPH orthogonal cutting simulation of A2024-T351 alloy. Procedia CIRP 8:152–157.